Novel Approach for Modeling the Dynamics of Fiber Breakage in Polymer Matrix Composites during Capillary Extrusion

F. SPORLEDER

Department of Chemical Engineering, Norwegian University of Science and Technology, Trondheim, Norway

J. M. CARELLA

Polymer Engineering and Science Group, National Research Institute of Materials Science and Technology (INTEMA), National Scientific and Technical Research Council (CONICET), National University of Mar del Plata (UNMdP), Mar del Plata, Argentina

C. A. DORAO

Department of Energy and Process Engineering, Norwegian University of Science and Technology, Trondheim, Norway

L. N. LUDUEÑA

Composite Materials Group (CoMP), National Research Institute of Materials Science and Technology (INTEMA), National Scientific and Technical Research Council (CONICET), National University of Mar del Plata (UNMdP), Mar del Plata, Argentina

Correspondence to: L. N. Ludueña; e-mail: luduenaunmdp@gmail.com.

Received: May 15, 2015
Revised: October 2, 2015
Accepted: October 27, 2015

ABSTRACT: In this work, a population balance equation (PBE) model is used to predict the evolution of the fiber breakage in thermoplastic polymer/short-fiber composites during capillary extrusion. The least squares spectral method was used to solve the resulting integrodifferential equation. The differences found between the experimental and simulated data were attributed to the selected breakage and redistribution functions. An experimental setup is proposed to find accurate breakage functions for this problem. The results indicate that the application of the PBE for such a breakage process could be a powerful tool for the design of injection molding molds. © 2015 Wiley Periodicals, Inc. Adv Polym Technol 2015, 0, 21635; View this article online at wileyonlinelibrary.com. DOI 10.1002/adv.21635

KEY WORDS: Composites, Computer modeling, Extrusion, Fiber, Injection molding, Thermoplastics

Introduction

Thermoplastic polymers are often reinforced by blending them with fibers of higher Young's modulus. Although Young's modulus for mostly used engineering thermoplastics are in the range of 1000–5000 MPa, for fibers this parameter may be up to three orders of magnitude higher.[1] Fibers that are not compatible need to be mechanically bonded to the thermoplastic with efficient surface compatibilizers that reduce the polymer–fiber interfacial energy increasing adhesion.[2] In this manner, the reinforcing effect is effective depending on the modulus, length, aspect ratio and volume ratio of the fibers and compatibilizer efficiency.

Many high performance products are made with thermoplastic/fiber composites by injection molding processes.[3] Automobile interior and exterior parts are injected with fiber-reinforced thermoplastics to reduce costs, seeking for long service life under the automobile hood, exposed to heat, steam and oil. Several aircraft parts are also injected with fiber-reinforced polyamides, polypropylenes and polyesters.[4]

For a given polymer/fiber system with fixed reinforcement volume fraction, the performance of the composite material depends mainly on the final fibers aspect ratio and orientation.[5]

Contract grant sponsor: Research Council of Norway. Contract grant number: YGGDRASIL scholarships 2011, Project Number 202825. Contract grant sponsor: National Agency of Science and Technology (ANPCyT). Contract grant number: PICT06 1560, Fonarsec FSNano004. Contract grant sponsor: National University of Mar del Plata (UNMdP). Contract grant number: 15G327.

The shear forces induced in injection molding produce fibers breakage that detriments the final mechanical properties of the material. In the case of the automobile industry, recycled materials are often used and further fiber breakage takes place.[6] Therefore, the prediction of the evolution of the topology of the fibers during the molding process is a critical aspect for obtaining an optimal final product.

It may be considered that one of the main contributions for fiber rupture during injection molding is the screw rotation during the melting of the polymer composite prior to injection. However, the fiber breakage at this stage can be characterized and its magnitude will be independent of the mold used. Many mold designs can be used with the same injection molding machine. In the case of molds, runners are the critical zones where fiber breakage takes place, since the shear forces are stronger due to the small cross-sectional area. Considering steady, incompressible, fully developed, and isothermal polymer flow along a runner with circular cross-sectional area, the shear force at wall at a given flow rate depends on R^{-4}, where R is the runner radius.[7] Therefore, capillary extrusion rheometry is useful to simulate flowing conditions inside injection molding runners. Figure 1 illustrates this explanation. Benhadou et al.[8] proposed this idea, suggesting that the fiber breakage process inside the mold runners (Fig. 1a) can be easier studied from capillary extrusion (Fig. 1b).

Experimental analysis and modeling of the fiber breakage during the flow of polymers in capillary flow have been reported in the literature.[9–13] Models are focused on the effect of the flow field on the buckling resistance of the fibers.[11] However, the flow field changes with the topology of the fibers, i.e., the evolution of the distribution of the length of the fibers locally affect the viscosity of the system and hence the flow field. Moreover, the buckling resistance of the fibers depends also on their aspect ratio and on the orientation of the fiber[11] and these parameters are modified throughout the process. Viscous heat generation and the non-Newtonian nature of polymers must also be taken into account.[7] In summary, the models available in the literature are not able to predict the evolution and the final topology of fibers flowing along a capillary. A model including all these parameters would minimize experimental trial and error steps in the preparation polymer/fiber composite materials with the expected properties. In addition, it would enhance the efficiency for mold designing in comparison with those models or experimental information that only deals with the initial and final topology of the fibers. A model solving all these issues would be extremely valuable for the industry of injection-molded thermoplastic polymer fiber composite products.

In this work, we propose a first attempt to solve this problem. The fibers in the runners can be characterized as a population of entities that break as they move along the capillary. As such, the population balance equation (PBE)[14] can be used to study the evolution of the fibers. This equation makes a statistical description of the evolution of a group of entities, and it has been applied to a large variety of problems in physics, biology, chemistry and engineering, as reviewed by Ramkrishna[14] and Sporleder et al.[15] The PBE has not yet been used before to study fiber breakage processes of polymer/fiber composites. The PBE uses a density function as its main variable, defined as a function of time, physical coordinates, and internal coordinates. The latter are used to represent properties of the entities, such as size,

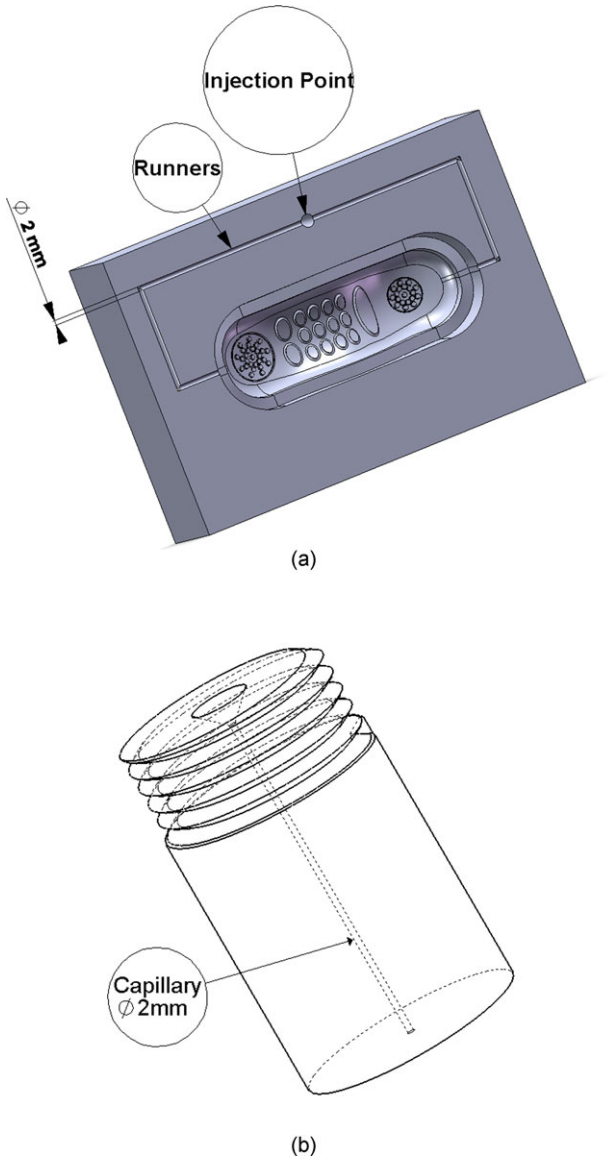

FIGURE 1. Schematic view for (a) cavity of a mold for injection molded telephone parts and (b) die used for capillary extrusion.

mass, temperature, composition, etc. For a dispersed phase case, the density function is affected by convection and by the death and birth of entities. In the case of fiber capillary extrusion, the latter are given by breakage events. The resulting equation is integrodifferential. Several methods have been proposed to solve this equation, as reviewed by Ramkrishna.[14] The great majority involves rewriting the PBE as a system of differential equations. Recently, Dorao et al.[16] have shown the applicability of the least squares method (LSM) to solve the PBE directly. Since then, the method and its spectral element version have been successfully applied to study droplets[17] and bubbly flow[18] using the PBE.

The aim of this work is to analyze the applicability of the PBE for predicting the evolution of the fiber breakage in polymer/short-fiber composite during capillary extrusion. The least squares spectral method will be used to solve the resulting integrodifferential equation. The numerical model will be validated with the experimental data obtained by George

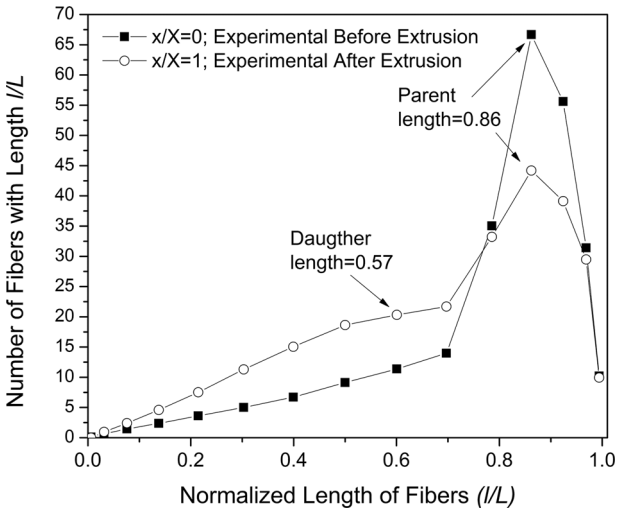

FIGURE 2. Fiber length distribution before and after extrusion. Interpolation of the experimental data set at 1640 s^{-1} reported by George et al.[22]

et al.[19] for capillary flow of short pineapple fiber reinforced low-density polyethylene composites. The main goal of this work is to show the evolution of a density function predicted with different breakage kernels and to compare the modeling results with experimental data. Four intrinsically different breakage kernels and two redistribution functions are tested. The effect of several combinations of them on the accuracy of the simulated results is analyzed.

Experimental data

This work is based on the experimental data reported by George et al.[19] They studied the melt rheological behavior of short pineapple fiber reinforced low-density polyethylene composites using an Instron capillary rheometer at different plunger speeds from 0.06 to 20 mm/min. Low density polyethylene (16MA 400) was obtained from Indian Petro Chemical Corporation Ltd, Vadodara. Pineapple leaf fibre (Ananus cosomus) was supplied by South India Textile Research Association, Coimbatore. The capillary used was made of tungsten carbide with an aspect ratio of 33.42 and an angle of entry of 90°C. The shear stress at wall (τ_W) was calculated using the Bagley correction. They measured the fiber length number distribution before and after extrusion at different shear rates ($\dot{\gamma}_W$=16.4, 164, and 1640 s^{-1}) by dissolving the polyethylene from the extrudate and measuring the fiber length using a travelling microscope. No data about the fiber content inside the composites and the extrusion temperature were presented in the work by George et al.[19] but these parameters are not significant for the aim of our work. The data set at 1640 s^{-1} was used to validate the simulations. This present set was chosen arbitrarily and only one set was used for the sake of simplicity.

Using interpolation, the whole space–size domain could be reconstructed for the experimental data, and the resulting normalized fiber length distribution is shown in Fig. 2.

The PBE: Theoretical Background

ONE-DIMENSIONAL, STEADY-STATE, CONSTANT VELOCITY, BREAKAGE-DOMINANT FORMULATION

The PBE allow us to describe the entities in a statistical manner by means of a density function *f(r,ξ,t)* defined such that *f(r,ξ,t)drdξ* represents the expected number of particles per unit volume in (r, $r+dr$) at time t, with the characteristic property of the particles ξ in (ξ, $\xi + d\xi$). The evolution of this density function must take into account the different processes that control the particle population such as breakage, coalescence, growth, and convective transport of the particles. The resulting equation is a nonlinear partial integrodifferential equation, which requires to be solved by a suitable numerical method. A detailed discussion about population balances in general has been made by Ramkrishna[14] and Sporleder et al.[15] One of the simplest cases of the PBE is the one-dimensional, steady-state, constant velocity, breakage-dominant, and binary break formulation. In such a case, the PBE can be described as follows[20]:

$$U \times \frac{\partial f(x,\xi)}{\partial x} = -b(\xi,x) \times f(\xi,x) + 1/2 * \int_{\xi}^{\xi_{max}} h(\xi,s,x) \times b(s,x) \times f(s,x) \times ds \text{ in } \Omega \quad (1)$$

$$f(\xi) = f_0(\xi) \text{ on} \Gamma_0 \quad (2)$$

with $\Omega = [\xi_{min}\ ,\ \xi_{max}] \times [0\ ,\ X]$, where ξ_{min} and ξ_{max} are the minimum and maximum values of the characteristic property (for our case of study, ξ represents the normalized fiber length), X is the total length of the channel in which the evolution of the particles size is being analyzed, s is the length of the fiber at position x along the channel, and U the velocity of the fibers. Equation (2) contains the initial condition $f_0(\xi)$ of the problem that is applied on $\Gamma_0 = (\xi \in \partial\Omega: x = 0 \vee x = X)$. The left-hand side of Eq. (1) represents the change in the fiber length distributions along the channel. The right-hand side of Eq. (1) describes the breakage process in terms of a breakage rate function, $b(\xi, x)$, and a redistribution function, $h(\xi, s, x)$. The breakage rate gives the frequency for the splitting of particles, and the redistribution function describes the outcome of a split.

The first term on the right-hand side of the Eq. (1) gives us the loss of fibers in the population for a breakage process; thus, $b(\xi, x)$ is the breakage rate of the particles of type ξ at x.

The second term on the right-hand side of Eq. (1) denotes the change in the population due to the arrivals of new fibers with length ξ at x, according to the breakage redistribution function$h(\xi, s, x)$. The redistribution function is defined as follows:

$$h(\xi,s,x) \times d\xi = \frac{\text{Number of fibers of size } [\xi, \xi + d\xi] \text{ that appear in } x}{\text{Total number of fibers of size } s \text{ that break in } x} \quad (3)$$

By definition:

$$\int_0^s h(\xi, s, x) \times d\xi = 2 \tag{4}$$

for binary breakage.

The main challenge in the population balance framework is the determination of numerical or analytical correlations for the functions that dictate the statistical behavior of the particles ($b(\xi, x)$ and $h(\xi, s, x)$).

MODEL

General Aspects

In this work, the fibers breakage evolution during the flow of a polymer composite in capillary extrusion will be described in terms of the one-dimensional, steady-state, constant velocity, breakage-dominant, and binary break formulation of the PBE, represented by Eq. (1). Coalescence and growth terms are neglected assuming well-dispersed polymer/fiber composites. The breakage rate and the redistribution function are considered to be only dependent on the characteristic property ξ, which in this work represents the normalized length of the fibers:

$$\xi = l/L = \text{Length of fiber/Length of the longest fiber} \tag{5}$$

The domain for the characteristic property ξ defined by Eq. (5) is [0.1].

It must be taken into account that this case of study was not previously analyzed using PBE. Thus, the adaptation of the PBE demands its retuning usually leading to the need of a completely new model considering that the functions for the breakage rate, $b(\xi)$, and the redistribution function, $h(\xi, s)$, are unknown for this particular case.

Dimensionless Variables

For the PBE to become independent of the velocity of the particles, U (m/s), we introduce the following dimensionless variables:

$$\tilde{x} = \frac{x * \dot{\gamma}_W}{U} \tag{6}$$

where x (m) is the position along the capillary axis and $\dot{\gamma}_W$(s^{-1}) is the shear rate at the wall of the capillary. The numerical solution proposed (described in the following section) define $\tilde{x}$ in the domain [0.1]. The equation to be solved can be expressed as follows:

$$\frac{\partial f\left(\xi, \tilde{x}\right)}{\partial \tilde{x}} = -B(\xi) * f(\xi, \tilde{x}) + 1/2 * \int_{\xi}^{\xi_{max}} h(\xi, s) * B(s) * f(s, \tilde{x}) * d\mathrm{s} \,\mathrm{in}\, \Omega \tag{7}$$

$$f(\xi, \tilde{x}) = f_0(\xi) \,\mathrm{on}\, \Gamma_0 \tag{8}$$

where $f(\xi)$ represents the number of fibers of normalized length ξ, $B(\xi) = \frac{b(\xi)}{\dot{\gamma}_W}$ and $B(s) = \frac{b(s)}{\dot{\gamma}_W}$ are the dimensionless breakage rates, and $f_0(\xi)$ is the experimental distribution of ξ before extrusion also named as the distribution of ξ at position x/X=0. It must be taken into account that in this way Eq. (7) becomes case dependent on $\dot{\gamma}_W$.

Models for the Breakage Rate

The evolution of the fiber breakage in thermoplastic polymer/short-fiber composites during capillary extrusion has not been previously studied using a PBE approach. Models for the breakage kernel according to this case of study are not reported in the literature. So, we propose several empirical breakage models to show the effects on the evolution of the density function. The design of the breakage rate function is based on the fact that longer fibers travelling within a polymer flow along a pressurized capillary are easier to break.[11,12] Thus, we proposed $b(\xi)$ functions for which longer fibers will break faster. The resulting equations for the breakage rate can be represented as follows:

$$b_0(\xi) = k \tag{9}$$

$$b_1(\xi) = k * \xi \tag{10}$$

$$b_2(\xi) = k * \xi^2 \tag{11}$$

$$b_3(\xi) = k * \xi^3 \tag{12}$$

where k is a constant. The value of $k = 0.45$ was found by trial and error such that the evolution of fiber breakage was relatively well predicted. Thus, the k value was chosen arbitrarily for the particular case (processing parameters and material formulation) analyzed in this work. It should be noted that the aim of this work was to demonstrate that the PBE can be used for the prediction of fiber breakage in capillary flow but not to find breakage rate or redistribution functions for any other processing conditions. In future works, more accurate breakage rate functions will be found. Experimental data of the evolution of fiber breakage inside a capillary will be studied by capillary extrusion and injection molding. Injection molding molds will be designed to precisely control the processing parameters and the fiber breakage inside mold runners. The last section of this work shows a detailed explanation of the experimental setup. Knowing the fiber length distributions along the runner after the breakage process, the breakage rate function can be optimized solving the PBE inverse numerical problem. In such a case, the dynamics of fiber breakage will be the input for the simulations while the breakage kernel will be the unknown. Processing conditions and material formulation will be taken into account in the final PBE model.

Models for the Redistribution Function

Since the breakage function only gives us the probability for a fiber to break up, we still need the redistribution function to describe the size distribution of the daughter fibers being the outcomes of a breakage event. Redistribution functions for our case of study were not previously reported in the literature. For this reason, we adopted models that have been used for other physical problems that require the same constraints of this work: binary breakage, mass balance, and number balance for the particles. Marcheti et al.[21] studied several redistribution functions that mathematically satisfy these constraints. We selected the more appropriate model in terms of accuracy between the experimental and simulated results, and accurate prediction of the daughter fibers' length. For this analysis, it is important to note that the experimental results (see Fig. 2) show daughter fibers having two-thirds the length of the parent ones. Marchetti et al.[21] have reviewed several kernels for the size redistribution function in binary breakage. A normal distribution and a beta distribution function were adopted in this work:

$$h_1(\xi, s) = \frac{2.4}{s^3} * \exp\left(-\frac{4.5 * \left(2 * \xi^3 - s^3\right)^2}{s^6}\right) \tag{13}$$

$$h_2(\xi, s) = \frac{30}{s} * \left(\frac{\xi}{s}\right)^3 * \left(1 - \frac{\xi}{s}\right) \tag{14}$$

As was previously explained, these two equations fulfill the three constraints of the system: binary breakage, mass balance, and number balance for the particles.[21]

Numerical Method

The LSM was adopted to solve the actual problem. A detailed explanation of the application of LSM to the direct PBE was reported by Dorao and Jakobsen.[22] The basic idea in the LSM is to minimize the integral of the square of the residual over the computational domain. For the cases in which the exact solution is sufficiently smooth, the convergence rate is exponential by increasing the polynomial degree of the approximation. To solve Eq. (7) using the LSM, it is convenient to rewrite it using an operator form as follows:

$$\Im b = g \, in \, \Omega \tag{15}$$

where $\Im$ is the population balance operator and g is the term that does not depend on $B(\xi)$. They can be defined as:

$$\Im b = -B(\xi) * f(\xi, \widetilde{x}) + 1/2 * \int_{\xi}^{\xi_{\max}} h(\xi, s) * B(s) * f(s, \widetilde{x}) * ds \tag{16}$$

$$g = \frac{\partial f\left(\xi, \widetilde{x}\right)}{\partial \widetilde{x}} \tag{17}$$

The least squares formulation is based on the minimization of a norm-equivalent functional. This method consists of finding the minimizer of the residual in a certain norm. The norm-equivalent functional for the problem given by Eq. (15) is:

$$\wp(b) \equiv \frac{1}{2} * \| \Im b - g \|^2_{Y(\Omega)} \tag{18}$$

where Y is the residual space. In some cases, optimal convergence in the LSM can be achieved only if L_2 norms are used to define the least squares functional in Eq. (18).[23] Actually, in this work, the minimization is based on a L_2 norm, i.e., $\| \bullet \|^2_{Y(\Omega)} \equiv \| \bullet \|^2_{L_2(\Omega)}$. Hence, the norm is given as:

$$\|\bullet\|^2_{L_2(\Omega)} \equiv \langle \bullet, \bullet \rangle^2_{L_2(\Omega)} = \int_{\Omega} \bullet \cdot \bullet \, d\Omega \tag{19}$$

Based on variational analysis, the minimization statement is equivalent to:

Find $b \in Z(\Omega)$ such that

$$\lim_{\varepsilon \to 0} \frac{d}{d\varepsilon} \wp\left(b + \varepsilon \nu\right) = 0 \forall \nu \in Z\left(\Omega\right) \tag{20}$$

where $Z(\Omega)$ is the space of the admissible functions and ν is any noise or perturbation function. Consequently, the necessary condition can be written as:

Find $b \in Z(\Omega)$ such that

$$\mathrm{A}\left(b, \nu\right) = F\left(\nu\right) \forall \nu \in Z\left(\Omega\right) \tag{21}$$

with

$$\mathrm{A}\left(b, \nu\right) = \langle \Im b, \Im \nu \rangle_{L_2(\Omega)} \tag{22}$$

$$F\left(\nu\right) = \langle g, \Im \nu \rangle_{L_2(\Omega)} \tag{23}$$

where $\mathrm{A} : \mathrm{Z} \times \mathrm{Z} \to \Re$ is a symmetric, continuous bilinear form, and $\mathrm{F} : \mathrm{Z} \to \Re$ a continuous linear form provided that the $\Im$ operator is linear.

Finally, the discretization statement consists of seeking the solution in a reduced subspace, i.e., $\mathrm{b_N} \in Z_N(\Omega) \subset Z(\Omega)$. Then, assuming that $Z_N = \mathrm{span}\{\Phi_0, \Phi_1, ..., \Phi_N\}$ with $\Phi_l = \Phi_i \otimes \Phi_j$ constructed as the tensor product of one-dimensional basis functions, we obtain

$$\mathrm{b_N} = \sum_{l=0}^{N} b_l \Phi_l \tag{24}$$

where $\mathrm{b_l}$ are the coefficients for the expansion. In particular, the Lagrange interpolant polynomials throughout the Gauss–Lobatto and Gauss–Legendre–Lobatto quadrature points are used.

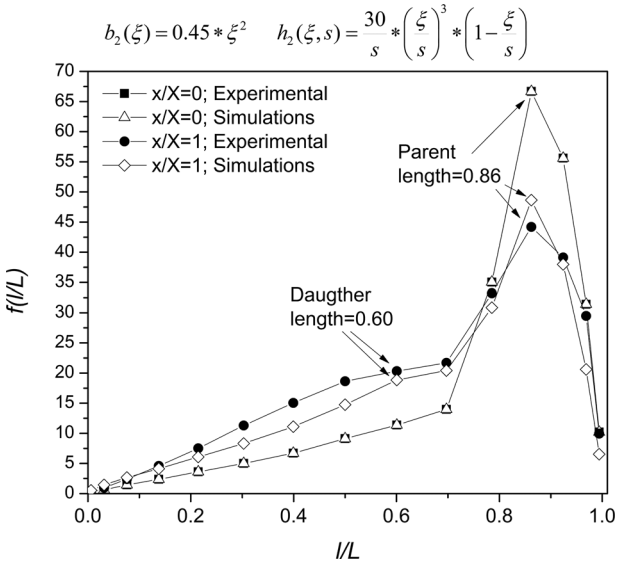

FIGURE 3. Experimental and simulated fiber length distributions before and after the breakage process during extrusion at 1640 s^{-1}.

Using approximation[21] in expression[18] and taking systematically $v = \Phi_i \forall i = 0, 1, ..., N$, we get

$$\mathrm{Ab} = F \tag{25}$$

where the matrix $\mathrm{A} \in \Re^{NxN}$ and vectors $\mathrm{b}, F \in \Re^N$ are defined as

$$[\mathrm{A}]_{\mathrm{ij}} = \mathrm{A}\left(\Phi_{\mathrm{j}}, \Phi_i\right) = \left\langle \Im\Phi_j, \Im\Phi_i \right\rangle_{L_2(\Omega)} \tag{26}$$

$$[F]_{\mathrm{i}} = F\left(\Phi_i\right) = \langle g, \Im\Phi_i \rangle_{L_2(\Omega)} \tag{27}$$

Results and Discussions

ANALYSIS OF SENSITIVITY OF THE MODEL OVER CHANGES IN THE BREAKAGE RATE AND THE REDISTRIBUTION FUNCTIONS

Figure 3 shows the experimental and simulated fiber length distributions before ($x/X = 0$, where x is the position along the capillary and X is its length) and after (x/X=1) the breakage process during extrusion at 1640 s^{-1}.

The breakage kernels used for this plot were $h = h_2$, $b = b_2$, and $k = 0.45$. The experimental and simulated curves before extrusion are superimposed since the experimental data before extrusion were the initial values for the simulations. It can be observed from Fig. 3 that the simulated results after extrusion satisfies binary breakage. The lengths of the parent (l/L=0.86) and the daughter (l/L=0.60) fibers after extrusion predicted by the simulations are also in good agreement with the experimental observations. This result is a consequence of the correct selection of the redistribution function. Analyzing the *f(l/L)* values after extrusion at fixed *l/L*, it can be observed that the number of these fibers (*f(l/L)*) was not exactly predicted. We can define an error ε between the modeled and the experimental distributions by using the differences between experimental and simulated *f(l/L)* values at fixed *l/L*. The mean value (ε_1) of this error can be calculated by the following equation:

$$\bar{\varepsilon_1}\,(\%) = \frac{\sum_{i=0}^{N} \varepsilon_i}{N} = \frac{\sum_{i=0}^{N} \left| \frac{f^{\exp}_{(l/L)_i} - f^{\mathrm{sim}}_{(l/L)_i}}{f^{\exp}_{(l/L)_i}} \cdot 100 \right|}{N} \tag{28}$$

where N is the number of points of the distribution and i is a counter for the position at each fiber length. This calculation is useful to estimate not only the accuracy of the simulations, but also to analyze the sensitivity of the model itself over changes in the breakage rate and redistribution functions.

The model used for the simulations in Fig. 3 was selected after analyzing the different combinations of the breakage rate and redistribution functions proposed. First, we calculated the ε_1 values corresponding to each b_i, h_i combinations. Table I shows the results.

The b_0 breakage kernel predicts a breakage rate independent of the fiber length. This case has not physical basis due to the fact that longer fibers of the same diameter are easier to brake as a consequence of their decreased resistance to shearing flow.[21] For this reason, the simulations corresponding to the combination [b_0; h_1] did not converge, while large error was obtained using b_0 and h_2. The optimal combination between the breakage rate and the redistribution function was [b_2; h_2]. The second analysis consisted of the calculation of an error based on the differences between the simulated and experimental daughter and parent fiber lengths. It can be seen in Fig. 3 that the daughter length cannot be accurately quantified since a peak in that zone is not clearly recognized. To solve this problem, the distributions after breakage (see Fig. 3) can be deconvoluted into two Gaussian functions in such a way that the sum of those Gaussian distributions fits the original fiber length distribution. We quantified the daughter and parent lengths by the position of the peaks of each Gaussian function. Figure 4 shows the deconvolution of the simulated fiber length distributions after the breakage process during extrusion at 1640 s^{-1}. The *x*-axis position of the peak corresponding to the Gaussian function located at shorter *l/L* values (daughter distribution shown in Fig. 4) represents the daughter length while the one at longer *l/L* values (parent distribution shown in Fig. 4) corresponds to the parent length. The accuracy between the experimental and the predicted daughter and parent lengths after extrusion at 1640 s^{-1} was calculated by the following equations:

$$\varepsilon_2\,(\%) = \frac{(l/L)^{\mathrm{daugther\,exp}} - (l/L)_i^{\mathrm{daughersim}}}{(l/L)^{\mathrm{daugther\,exp}}} \cdot 100 \tag{29}$$

$$\varepsilon_3\,(\%) = \frac{(l/L)^{\mathrm{parent\,exp}} - (l/L)_i^{\mathrm{parent\,sim}}}{(l/L)^{\mathrm{parent\,exp}}} \cdot 100 \tag{30}$$

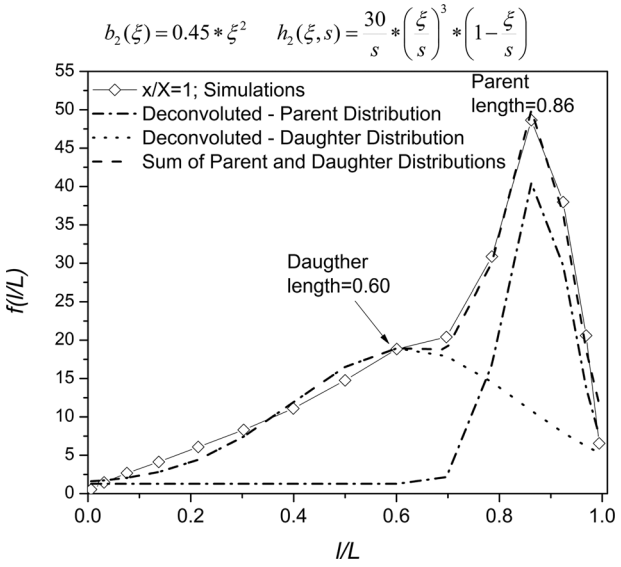

FIGURE 4. Deconvolution of the simulated fiber length distribution after the breakage process during extrusion at 1640 s^{-1}.

Table II reports the values of ε_2 and ε_3 for each breakage rate–redistribution function combination. The breakage rate functions b_0 and b_1 were not useful for predicting the daughter and parent fiber length after the breakage process. This result is in accordance with the previous analysis based on $\bar{\varepsilon_1}$. On the other hand, b_2 and b_3 accurately predicted these characteristics of the distributions for both redistribution functions. Based on the analysis of the errors proposed, it can be concluded that $[b_2; h_2]$ was the best combination for the simulation of this case of study. The corresponding curves are previously shown in Fig. 3.

Another feature that must be analyzed is the sensitivity of the model over variations in the breakage rate. This analysis demonstrates the suitability of the model for the physical problem proposed. For example, a variation of 10% in the breakage rate should not have significant effect on $\bar{\varepsilon_1}$. We run simulations using $k = 0.405$, $k = 0.45$, and $k = 0.495$ for each breakage rate function. This analysis was done for both redistribution functions proposed in this work. Table III shows the values of $\bar{\varepsilon}_1$ for each breakage rate–redistribution function combination.

It can be observed that except to the breakage rate model b_0, varying ±10% the value of k (see Eqs. (9)–(12)) did not significantly change the ε_1 values for any of the $[b_i; h_i]$ combinations analyzed.

These results demonstrates that the model is not sensitive to small changes in the constants of the breakage rate models proposed. Moreover, it can be concluded that the PBE model proposed is suitable for the physics of this case of study.

As was previously demonstrated, $[b_2; h_2]$ was the best combination between those analyzed in this work but the obtained $\varepsilon_1 = 13\%$ should be reduced for better fitting of the experimental fiber length distribution after the breakage process. In future works, experimental tests will be performed characterizing the initial and final fiber size distribution after a breakage process in a capillary extrusion rheometer. Injection molding molds will be also designed to precisely control the processing parameters and the fiber breakage inside a mold runner. In such tests, the polymer/short-fiber composite will flow along a circular channel with known geometry by the action of a controlled pressure gradient and temperature. The details of the experimental design is shown in the last section of this work. With these parameters, knowing the rheology of the system, the shear stress at wall of the runner can be calculated. The initial and final fiber size distribution will be characterized for solving the inverse PBE problem finding more accurate breakage rate functions to obtain more precise fitting. The work will be focused in including the shear stress magnitude at wall in the k parameter of the breakage rate

TABLE I
Error (ε_1 (%)) Calculated from the Simulated and Experimental Results for Each Breakage Rate–Redistribution Function Combination

	Redistribution Function	
Breakage Rate Function	$h_1(\xi, s) = \frac{2.4}{s^3} * \exp\left(-\frac{4.5*(2*\xi^3 - s^3)^2}{s^6}\right)$	$h_2(\xi, s) = \frac{30}{s} * (\frac{\xi}{s})^3 * (1 - \frac{\xi}{s})$
$b_0 = 0.450$	Not converging	59
$b_1 = 0.450 * \xi$	Not converging	15
$b_2 = 0.450 * \xi^2$	18	13
$b_3 = 0.450 * \xi^3$	22	16

TABLE II
Error ($[\varepsilon_2; \varepsilon_3]$ (%)) Calculated from the Simulated and Experimental Daughter and Parent Fiber Lengths for Each Breakage Rate–Redistribution Function Combination

	Redistribution Function	
Breakage Rate Function	$h_1(\xi, s) = \frac{2.4}{s^3} * \exp\left(-\frac{4.5*(2*\xi^3 - s^3)^2}{s^6}\right)$	$h_2(\xi, s) = \frac{30}{s} * (\frac{\xi}{s})^3 * (1 - \frac{\xi}{s})$
$b_0 = 0.450$	Not converging	Not Converging
$b_1 = 0.450 * \xi$	Not converging	[17;0]
$b_2 = 0.450 * \xi^2$	[0;0]	[0;0]
$b_3 = 0.450 * \xi^3$	[0;0]	[0;0]

TABLE III
Analysis of the Sensitivity of the Model over Changes in the Breakage Rate Function

	Redistribution Function	
Breakage Rate Function	$h_1(\xi, s) = \frac{2.4}{s^3} * \exp\left(-\frac{4.5*(2*\xi^3-s^3)^2}{s^6}\right)$	$h_2(\xi, s) = \frac{30}{s} * (\frac{\xi}{s})^3 * (1 - \frac{\xi}{s})$
$b_0 = 0.405$	Not converging	47
$b_0 = 0.450$	Not converging	59
$b_0 = 0.495$	Not converging	71
$b_1 = 0.405 * \xi$	Not converging	12
$b_1 = 0.450 * \xi$	Not converging	15
$b_1 = 0.495 * \xi$	Not converging	18
$b_2 = 0.405 * \xi^2$	18	13
$b_2 = 0.450 * \xi^2$	18	13
$b_2 = 0.495 * \xi^2$	18	15
$b_3 = 0.405 * \xi^3$	23	17
$b_3 = 0.450 * \xi^3$	22	16
$b_3 = 0.495 * \xi^3$	21	16

The values reported in each cell correspond to ε_1 (%).

function, which would allow using the same model for different processing parameters (pressure gradient and mold temperature) and different channel geometries.

PREDICTION OF THE EVOLUTION OF THE FIBER BREAKAGE ALONG THE CAPILLARY AXIS

The prediction of the evolution of the fiber length distribution during the flow of polymer/fiber composite materials along the injection molding molds runners is valuable information that has not been studied before. These results can be used as a powerful tool for designing injection molding molds to obtain an injected polymer/fiber composite product with the desired properties. This tool may save time and money that is often spent on trial and error attempts. Figure 5 shows the simulated results for capillary extrusion, which is analogous to the flow inside the runners.

Figures 5a and 5b clearly show the reduction of the number of parent fibers and the born of daughter fibers with length two-thirds of the parent ones as a function of the position along the capillary. Both conditions binary breakage and daughter fibers with length two-thirds of their initial value were conserved all along the capillary, as was expected from the previous analysis. This result suggests that independently of the shear stress magnitude, the residence time of the polymer/short-fiber system flowing inside the capillary is an important parameter to take into account.

FUTURE WORKS: EXPERIMENTAL SETUP FOR PBE OPTIMIZATION

It was demonstrated that the PBE model is applicable for a fiber breakage process in capillary flow. In the case of injection molding, the fiber breakage in the injection screw section is critical and difficult to be avoided. On the other hand, the simulation of the breakage process inside the injection runners using a PBE model can prevent further undesirable breakage levels. We are actually designing an experimental setup to study the fiber breakage dynamics in injection molding runners at controlled flowing conditions. The dynamics of fiber length distribution will be measured avoiding the fiber breakage occurring at the injection screw section. Figure 6 shows a schematic view of the mold. The following steps will be performed to acquire the necessary experimental data:

1. One weight percent polymer/fiber composites will be prepared by melt blending in a brabender type mixer at low screw rotation speed. Low fiber contents will be used to minimize fiber/fiber interactions. Low screw rotation speed will be used to avoid significant fiber breakage during blending process.
2. Two-millimeter thick sheets will be prepared by compression molding.
3. Fiber length distribution inside the sheets will be characterized by burning the polymer and measuring the fiber length in scanning electron or optical microscopy. This results will be used as the initial conditions for the simulations.
4. Sheets will be placed in the first cavity as shown in Fig. 6. A pressure sensor is placed in this cavity.
5. The first cavity will be heated until melting of the sheet inside of it is achieved.
6. The sheet inside the first cavity is pushed by the injection of pure polymer.
7. Molten polymer/composite in the first cavity is forced to flow along the runner shown in Fig. 6. The pressure drop along this runner is measured. The geometry of the runner and the rheology of the composite at the processing conditions are known. Therefore, the fiber length distribution in a cross-sectional area at different axial positions along the runner can be measured as a function of the shear stress at wall.

Using this experimental information, the inverse PBE problem will be solved and the k parameter of the breakage rate function will be optimized becoming the breakage rate independent of the processing conditions.

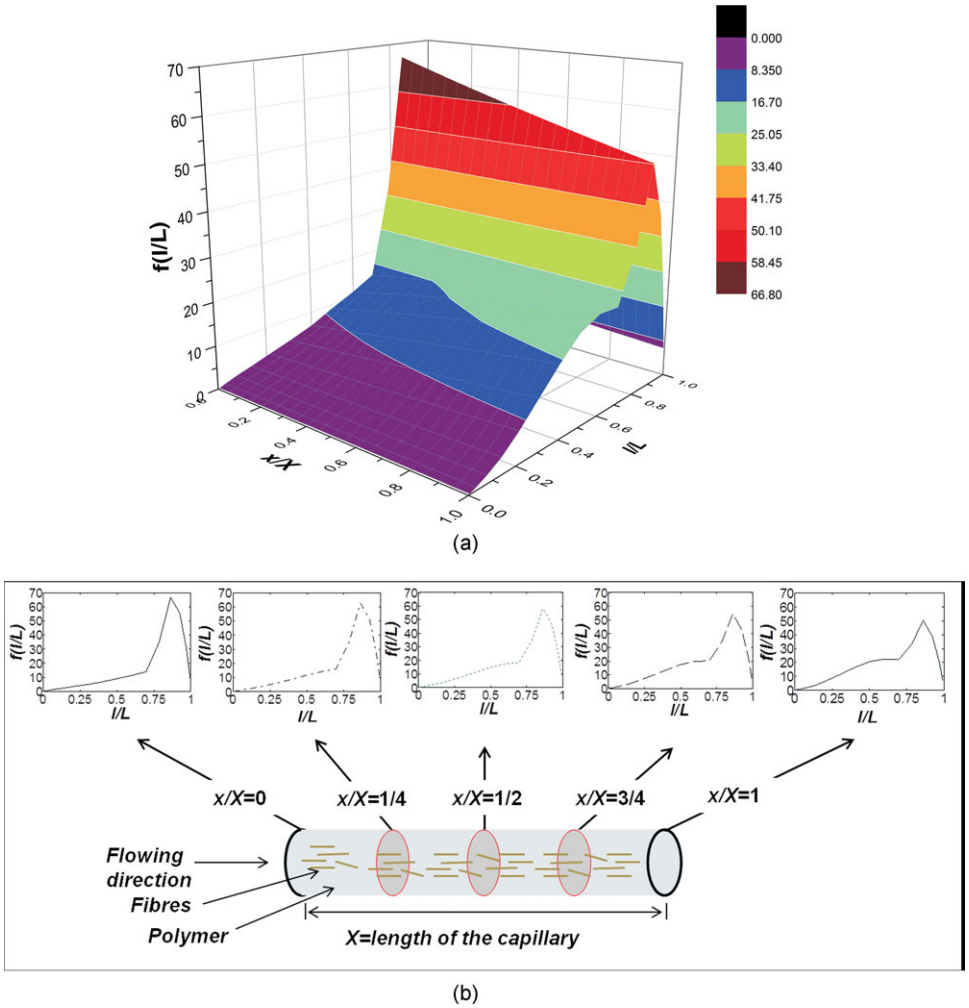

FIGURE 5. Simulations of the evolution of the fibers topology: (a) 3D graphic and (b) schematic view of the flowing composite along the capillary showing the simulated distribution of fiber length at several positions.

1) Injection point (pure polymer)

2) First cavity. Pressure sensor.

3) Composite is pushed by pure polymer and fibers breakage ocurrs along this runner

4) Second cavity is used as reservoir

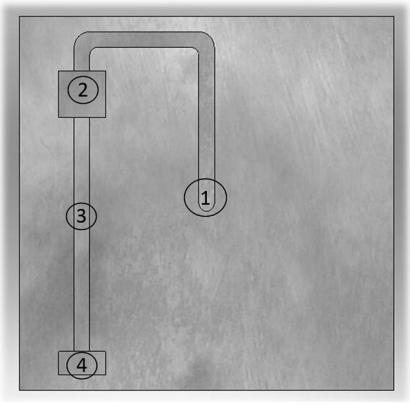

FIGURE 6. Schematic view of the mold to be used for the experimental work designed for finding a PBE model including material formulation and processing conditions.

Conclusions

The PBE was successfully adapted to simulate the evolution of the fiber length distribution during the breakage process of polymer/short-fiber composites flowing inside an extrusion capillary. The least squares spectral method was applied for solving the partial integrodifferential model. The problem was simplified to a one-dimensional, steady-state, constant velocity, breakage-dominant, and binary break formulation. The model derived describes the breakage regardless of the physics of the problem, as it can be assumed to be the sum of the breakage effects due to turbulence, shear, segregation, etc. The modeling concept proposed in this work was not previously reported in the literature. So, further work was required to establish a link between the model and the physical characteristics of the system. Different empirical breakage rate models were proposed and redistribution functions, which were previously used in other physical problems, were adapted for our particular case of study.

It was demonstrated that the evolution of the dispersed phase was strongly dependent on the models used for the breakage phenomena. The obtained results indicate that the application of the PBE for such a breakage process can also be extrapolated to other processing techniques such as injection molding. In future works, an experimental setup will be designed to validate the simulated breakage process along injection molding runners and also to solve the inverse PBE problem to optimize the breakage rate function. This work has technological importance since it can be used as a powerful tool for the design of dies and molds for melt processing of high-performance thermoplastic polymer/short-fiber composite products, saving costs and time that are often spent in trial and error steps.

References

1. Baillie, C. In Green Composites: Polymer Composites and the Environment; Nishino, D. T. (Ed.); Woodhead Publishing, 2004; pp. 49–80.
2. Zhuang, R.; Burghardt, T.; Mäder, E. Compos Sci Technol 2010, 70, 1523.
3. Pantani, R.; Coccorullo, I.; Speranza, V.; Titomanlio, G. Prog Polym Sci 2005, 30, 1185.
4. Biron, M. In Thermoplastics and Thermoplastic Composites; Ed. M. Biron, Elsevier: Oxford, 2007; pp. 33–153.
5. Wang, J.; Geng, C.; Luo, F.; Liu, Y.; Wang, K.; Fu, Q.; He, B. Mater Sci Eng A 2011, 528, 3169.
6. Bernasconi, A.; Rossin, D.; Armanni, C. Eng Fract Mech 2007, 74, 627.
7. Tadmor, Z., Gogos, C. Principles in Polymer Processing, 2nd ed.; Wiley, New Jersey, 2006.
8. Benhadou, M.; Haddout, A.; Villoutreix, G. J Reinf Plast Compos 2007, 26, 1357.
9. Czarnecki, L.; White, J. J Appl Polym Sci 1980, 25, 1217.
10. Fisa, B. Polym Compos 1985, 6, 232.
11. Franzén, B.; Klason, C.; Kubát, J.; Kitano, T. Composites 1989, 20, 65.
12. Mittal, R.; Gupta, V.; Sharma, P. Compos Sci Technol 1998, 31, 295.
13. Schweizer, R. Polym Plast Technol Eng 1982, 18, 81.
14. Ramkrishna, D. In Population Balance—Theory and Applications to Particulate Systems in Engineering; Press, A., (Ed.); Academic Press, San Diego, CA, USA, pp. 117–192, 2000.
15. Sporleder, F.; Borka, Z.; Solsvik, J.; Jakobsen, H. Rev Chem Eng 2012, 28, 149.
16. Dorao, C.; Jakobsen, H. Chem Eng Sci 2006, 61, 5070.
17. Patruno, L.; Dorao, C.; Dupuy, P.; Svendsen, H.; Jakobsen, H. Chem Eng Sci 2009, 64, 638.
18. Sporleder, F.; Dorao, C.; Jakobsen, H. Chem Eng Sci 2011, 66, 3133.
19. George, J.; Janardhan, R.; Anand, J.; Bhagawan, S.; Thomas, S. Polymer 1996, 37, 5421.
20. Dorao, C.; Lucas, D.; Jakobsen, H. Appl Math Modell 2008, 32, 1813.
21. Marchetti, J.; Patruno, L.; Jakobsen, H.; Svendsen, H. Chem Eng Sci 2010, 65, 5881.
22. Dorao, C.; Jakobsen, H. Comput Chem Eng 2006, 30, 535.
23. Bochev, P., Gunzburger, M. In Least-Squares Finite Element Methods, 1st ed.; Springer: Heidelberg, Germany, 2009.